COMPDYN 2011
III ECCOMAS Thematic Conference on
Computational Methods in Structural Dynamics and Earthquake Engineering
M. Papadrakakis, M. Fragiadakis, V. Plevris (eds.)
Corfu, Greece, 25–28 May 2011

NONLINEAR ANALYSIS OF R/C PANELS BY A TWO PARAMETER CONCRETE DAMAGE MODEL

L. Tesser[1], F.C. Filippou[2], D.A. Talledo[3], R. Scotta[1], R. Vitaliani[1]

[1] University of Padua – Dept. of Structural and Transportation Engineering
Via Marzolo, 9 – 35131 Padua, ITALY
tesser@dic.unipd.it

[2] University of California at Berkeley – Dept. of Civil and Environmental Engineering
760 Davis Hall – 94720 Berkeley CA, USA
filippou@ce.berkeley.edu

[3] University IUAV of Venice
Terese – Dorsoduro 2206 – 30123 Venice, ITALY
talledo.diego@gmail.com

Keywords: reinforced concrete panel, membrane model, nonlinear analysis, damage model

Abstract. *The paper prosents an efficient numerical model for the inelastic response analysis of R/C panels under cyclic excitations. A plane stress 2d membrane model has been developed that accounts for the concrete and reinforcing steel interaction. The reinforcing bars are modeled as multiple smeared steel layers with an uniaxial stress-strain relation in the bar direction following the Menegotto-Pinto constitutive model with isotropic hardening. The concrete material model is based on damage mechanics with an efficient two parameter damage law. At this stage of the research the bond-slip between concrete and rebars is not taken into account.*

The new model is validated by comparison with several experimental results on reinforced concrete panels from the literature. The tests are carried out under quasi-static conditions. The accuracy of the model in reproducing the cyclic behavior of reinforced concrete panels with different reinforcement ratio and bar inclination is excellent.

1 INTRODUCTION

Reinforced concrete (R/C) panels are commonly used in the lateral force resisting system of structures in seismic risk zones for serviceability, ultimate strength and ductility considerations. They are either used alone or are coupled with moment resisting frames to resist the lateral forces.

The assessment of the behavior of R/C panels have been the focus of important analytical and experimental investigations aiming to evaluate the strength and particularly the shear transfer across the cracks [1–4].

The necessity of assessing advanced performance levels in high seismic zones has encouraged the research towards a deeper understanding on the nonlinear cyclic behavior of the R/C panels [5–9].

All the while many investigations on nonlinear analysis of R/C panels by finite element methods have been carried out. The available studies are not reviewed here in details, nonetheless, in the opinion of the authors, they can be subdivided into two categories: some researchers developed very sophisticated models while others searched for simplified ones as it is clarified below.

The works of the first category focus their attention on addressing the general two-dimensional problem, by means of R/C nonlinear constitutive models belonging to the different frameworks; i.e. elasto/viscoplasticity [10–12], fracture theory [13, 14], continuum damage mechanics [15–17], smeared crack models [18], modified compression field theory [19–21], softened membrane models [22].

Some of the cited works found their way into modern computer codes, but they often turn out to be rather complex or excessively expensive from the computational point of view, especially if applied to large scale structures.

The models in the second category are less general and they are addressing specific problems as beam-column joint panel [23], macroscopic fiber based model for shear walls [24, 25] or enhanced beam model [26, 27]. These models are suitable for large scale structures but they can be applied only for moderate shear demand since they do not address all the physical issues in the case of significant biaxial membrane stresses. Because of these limitations, the use of such nonlinear methods for the R/C panel design and assessment do not seem to meet the challenges of the earthquake engineering practice.

The purpose of the present study is the development of a membrane model for R/C panels addressing the evaluation of strength and ductility under cyclic loading. The proposed model belongs to the first model category while being suitable for the analysis of large scale structures. The membrane under plane stress state conditions is defined by superposition of distinct concrete and reinforcing steel material models. The model takes into account only the axial response of the reinforcing bars [28]. The bond slip effects are not taken into account at the present stage as well as the stiffness and strength of the bars perpendicularly to their alignment. The selection of the damage mechanics as framework for the concrete constitutive law comes from its ability in describing concrete behaviors avoiding excessive complications in the numerical procedure for the material state determination. In order to study the cyclic behavior of concrete panels subjected to shear loading, it is necessary to introduce two damage parameters, that account for the two different concrete failure modes in tension and in compression [16, 28]. The model of Faria et al. [29], although notably efficient, was developed for massive concrete structure such as dams in which the influence of the plastic strain in tension is supposed to be very low. Thus the simplified plastic evolution law, that disregards the plastic strains for tensile stresses, cannot capture the progressive crack opening typical of a cyclic loading of R/C panels. A more general plastic evolution law, that is more accurate for plane

stress state problem, is proposed to reproduce the plastic strains for general stress configurations.

For what concerns the reinforcing steel material, the simulation of the Baushinger effect is important to estimate the dissipated energy in hysteretic cycles precisely. Thus the model of Menegotto-Pinto with isotropic hardening developed by Filippou et al. [30] is profitably used.

2 CONCRETE DAMAGE MODEL

2.1 The model fundamentals

The proposed concrete constitutive law belongs to the class of energy-based isotropic continuum damage models. The model presented in this work takes into account both tensile and compressive concrete failure modes, by means of two damage parameters, and also the microcrack opening and closing, by considering the spectral decomposition of the stress tensor.

The damage and plastic unloading processes are assumed to be elastic. Reference is made to the paper of Ju [31] for the detailed explanation of the elastoplastic damage model framework and the adopted notations.

The split of the total strain tensor into "elastic-damage" and "plastic-damage" parts is assumed:

$$\boldsymbol{\varepsilon} = \boldsymbol{\varepsilon}^e + \boldsymbol{\varepsilon}^p \tag{1}$$

The locally averaged free energy potential is postulated according to the work of Faria et al. [29]:

$$\begin{aligned}\Psi(\boldsymbol{\varepsilon}, \boldsymbol{\varepsilon}^p, d^+, d^-) &= (1-d^+)\Psi_0^+(\boldsymbol{\varepsilon}, \boldsymbol{\varepsilon}^p) + (1-d^-)\Psi_0^-(\boldsymbol{\varepsilon}, \boldsymbol{\varepsilon}^p) = \\ &= (1-d^+)\frac{1}{2}\overline{\boldsymbol{\sigma}}^+ : \boldsymbol{\varepsilon}^e + (1-d^-)\frac{1}{2}\overline{\boldsymbol{\sigma}}^- : \boldsymbol{\varepsilon}^e\end{aligned} \tag{2}$$

where d^+, d^- represent the positive and negative damage parameters respectively and $\overline{\boldsymbol{\sigma}}^+$, and $\overline{\boldsymbol{\sigma}}^-$ are the positive and negative part of the effective stress tensor defined by:

$$\overline{\boldsymbol{\sigma}} \equiv \mathbf{C}^0 : \boldsymbol{\varepsilon}^e \tag{3}$$

where $\mathbf{C}^0$ is the fourth-order elastic stiffness tensor.

During any physical process the energy dissipation shall be always non-negative in agreement with the first thermodynamic principle. This condition is expressed by the following Clausius-Duhem inequality that holds for any admissible process:

$$\dot{\boldsymbol{\varepsilon}} : \left[\boldsymbol{\sigma} - \frac{\partial \Psi}{\partial \boldsymbol{\varepsilon}}\right] - \left[\frac{\partial \Psi}{\partial d^+} : \dot{d}^+ + \frac{\partial \Psi}{\partial d^-} : \dot{d}^-\right] - \frac{\partial \Psi}{\partial \boldsymbol{\varepsilon}^p} : \dot{\boldsymbol{\varepsilon}}^p \geq 0 \tag{4}$$

With the total strain a free variable, the term within the first square brackets shall be always zero. Thus the definition of the relation between the Cauchy stress tensor and the effective stress tensor can be obtained:

$$\begin{aligned}\boldsymbol{\sigma} = \frac{\partial \Psi}{\partial \boldsymbol{\varepsilon}} = \frac{\partial \Psi}{\partial \boldsymbol{\varepsilon}^e} = (1-d^+)\frac{\partial \Psi_0^+}{\partial \boldsymbol{\varepsilon}^e} + (1-d^-)\frac{\partial \Psi_0^-}{\partial \boldsymbol{\varepsilon}^e} = (1-d^+)\overline{\boldsymbol{\sigma}}^+ + (1-d^-)\overline{\boldsymbol{\sigma}}^- = \\ = (\mathbf{I} - \mathbf{D}) : \overline{\boldsymbol{\sigma}}\end{aligned} \tag{5}$$

The second and the third terms of the Equation (4) provide the damage and the plastic dissipation inequalities:

$$-\frac{\partial \Psi}{\partial d^+} : \dot{d}^+ - \frac{\partial \Psi}{\partial d^-} : \dot{d}^- = -\frac{\partial \Psi}{\partial \boldsymbol{d}} : \dot{\mathbf{d}} \geq 0 \tag{6}$$

$$-\frac{\partial \Psi}{\partial \boldsymbol{\varepsilon}^p} : \dot{\boldsymbol{\varepsilon}}^p \geq 0 \tag{7}$$

The reader is referred to the work of Faria et al. [29] that contains the demonstration of the validity of these inequalities.

Starting from the stress-strain relation of Equation (5), the fourth-order damage tensor $\mathbf{D}$ can be defined by the following expression [32]:

$$\mathbf{D} = \mathrm{d}^+\mathbf{P}^+ + \mathrm{d}^-\mathbf{P}^- \tag{8}$$

with $\mathbf{P}^+$ and $\mathbf{P}^-$ standing for the fourth-order projection tensors, positive and negative respectively, that have the following definitions:

$$\boldsymbol{P}^+ = \sum_i H(\bar{\sigma}_i)\, \boldsymbol{p}_i \otimes \boldsymbol{p}_i \tag{9}$$

$$\boldsymbol{P}^- = \boldsymbol{I} - \boldsymbol{P}^+ \tag{10}$$

where H is the Heaviside step function, $\bar{\sigma}_i$ is the i-th principal stress of the effective stress tensor $\bar{\boldsymbol{\sigma}}$ and $\boldsymbol{p}_i$ stands for the associated principal direction.

Then developing the Equation (6), the energy dissipated by the damage process shall be defined. The thermodynamic force, also called damage energy released rate, is expressed as:

$$-\boldsymbol{Y} = \frac{\partial \Psi}{\partial \boldsymbol{d}} \tag{11}$$

The damage energy release rate characterizes the damage evolution taking into account the progressive degradation of the mechanical properties of the material.

For the damage criteria, the damage energy release rate functions are defined with the following formulas:

$$Y^+ = \sqrt{E^0 \bar{\boldsymbol{\sigma}}^+ : \mathbf{C}^{0\,-1} : \bar{\boldsymbol{\sigma}}^+} \tag{12}$$

$$Y^- = \sqrt{3}(K\bar{\sigma}_{oct}^- + \bar{\tau}_{oct}^-) \quad or \quad Y^- = \sqrt{3}\left(KI_1 + \sqrt{J_2}\right) \tag{13}$$

where $\bar{\sigma}_{oct}^-$ and $\bar{\tau}_{oct}^-$ are the octahedral normal and shear stresses respectively (while I_1 and J_2 are the first invariant of the effective stress tensor and the second invariant of the deviatoric effective stress tensor), E^0 is the concrete Young modulus and K is a material property that accounts for the increase of compressive strength due to biaxial compression [29].

The energy release rate functions have also been called equivalent effective stresses $\bar{\tau}^+$ and $\bar{\tau}^-$ since they provide two scalar measures of the effective stress tensor [29].

With respect to the work in [29], the negative equivalent stress is defined slightly different so as to be homogeneous to the positive equivalent stress. As a result both the equivalent stresses have the same dimension of a stress component.

The damage threshold in uniaxial tension and uniaxial compression is described by variable r^+ and r^-, respectively, and they monitor the size of the expanding damage surface.

The numerical applications, carried out by the same authors, showed that the original damage criteria proposed by Faria et al. [29] agrees quite well with the experimental results for uniaxial, biaxial tension and biaxial compression stress states, whereas it has been demonstrated that improvements were necessary to better fit the experimental information for biaxial tension-compression states (see Figure 1).

A substantial improvement can be obtained by defining a unique damage criterion instead of two distinct ones in the earlier studies [29, 32].

Taking advantage from the homogeneity of the equivalent stresses, the following unique expression can adequately account for the interaction between tensile and compressive damage evolutions [36]:

$$g(Y^+, Y^-, r^+, r^-) = \left(\frac{Y^+}{r^+}\right)^2 + \left(\frac{Y^-}{r^-}\right)^2 - 1 \leq 0 \tag{14}$$

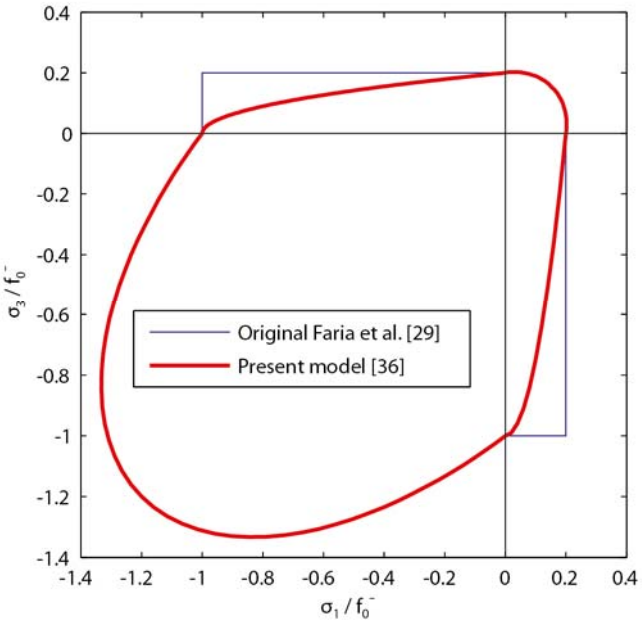

Figure 1: Initial elastic domain for plane stress states

The new damage criterion, that constitutes the damage surface, is superimposed to Faria's proposal in Figure 1.

It can be easily verified that, in the compression field ($Y^+ = 0$), the damage criterion becomes the modified Drucker-Pruger criterion and its suitability in representing biaxial stresses has been demonstrated by several studies [17, 29, 32].

In addition to the damage criterion the evolution of the damage threshold is determined by the following flow rule:

$$\dot{\boldsymbol{r}} = \dot{\gamma} \frac{\partial g(\boldsymbol{Y}, \boldsymbol{r})}{\partial \boldsymbol{Y}} \tag{15}$$

where γ is the damage consistency parameter. The relative Khun-Tucker conditions give:

$$g(\boldsymbol{Y}, \boldsymbol{r}) \leq 0 \qquad \dot{\gamma} \geq 0 \qquad \dot{\gamma} g(\boldsymbol{Y}, \boldsymbol{r}) = 0 \tag{16}$$

while the consistency condition is

$$\dot{\gamma} \dot{g}(\boldsymbol{Y}, \boldsymbol{r}) = 0 \tag{17}$$

The new damage threshold variables r can be computed with the Newton-Raphson method assuring the quadratic convergence of the material state determination.

It can be underlined that the elliptical shape of the damage criteria assures independent evolution of the positive and negative damage threshold for uniaxial tensile and compressive tests respectively.

In fact the tangent of the damage criteria is orthogonal to the normal vector when one of the thermodynamic forces is null.

Four parameters are needed to determine the initial damage surface: r_0^+ and r_0^- are the initial elastic damage thresholds for uniaxial tension and compression loadings respectively, K takes into account the additional strength under condition of biaxial compression and ν is the Poisson modulus.

Three common lab tests are necessary to compute the value of those parameters [29]: an uniaxial tension experiment, an uniaxial and a biaxial compression ones.

Using the Equation (12), the positive damage initial threshold is exactly equal to the concrete tensile strength, that is assumed to characterized the end of the elastic domain in the constitutive stress-strain relationship:

$$r_0^+ = f_0^+ = f_{ct} \tag{18}$$

Since the compressive constitutive law ends the linearity before reaching the peak strength, the uniaxial initial elastic limit f_0^- shall be evaluated from the uniaxial compression test leading to the corresponding negative damage threshold from the Equation (13):

$$r_0^- = \frac{\sqrt{3}}{3}\left(K - \sqrt{2}\right) f_0^- \tag{19}$$

From the results of a biaxial compression test, the biaxial compression elastic limit $f_{0,2D}^-$ can be obtained. Thus the parameter K, accounting for the increase of compressive strength due to biaxial compression, can be computed as

$$K = \sqrt{2}\frac{\left(f_{0,2D}^- - f_0^-\right)}{2f_{0,2D}^- - f_0^-} \tag{20}$$

The present constitutive model considers that damage criteria describes also the plastic surface so that the development of material damaging is simultaneous to the accumulation of irreversible strains for all the stress states.

Recalling the considerations of the work by Faria et al. [29] the following plastic evolution law is defined:

$$\dot{\boldsymbol{\varepsilon}}^p = \beta E^0 \frac{\langle \bar{\boldsymbol{\sigma}} : \dot{\boldsymbol{\varepsilon}} \rangle}{\bar{\boldsymbol{\sigma}} : \bar{\boldsymbol{\sigma}}} \mathbf{C}^{0^{-1}} : \bar{\boldsymbol{\sigma}} \tag{21}$$

having introduced β for the plastic strain coefficient.

It is clear that the plastic strain evolution proposes several simplifications with respect to the "effective stress space plasticity" [31] used to couple the damage evolution and the plastic flows in the spirit of obtaining a powerful tool for large time consuming seismic analyses.

In fact the adopted law determines the efficiency of the procedure. The presented choice leads to have the direction of the plastic strain rate parallel to those of the total strain rate. The effect is to introduce a simplification in the coupling between damage and plasticity and thus eliminating the additional iterative cycles inside the material state determination procedure. A consequent accepted limitation is a low efficacy in predicting the dilatancy of the concrete. In the cases in which the dilatancy plays an important role, the proposed model can be suitably applied taking care of choosing a different plastic potential.

The damage parameter evolution laws can be defined and they shape the concrete constitutive behavior. The analyses presented in this paper have been carried out using the laws proposed by Wu et al. [32].

The elastoplastic damage tangent modulus in the effective stress space can be derived from the previous expressions

$$\bar{\mathbf{C}}^{\mathrm{ep}} = \mathbf{C}^0 - \frac{\left(\mathbf{C}^0 : \boldsymbol{l}(\bar{\boldsymbol{\sigma}})\right) \otimes \left(\mathbf{C}^0 : \frac{\partial g}{\partial \bar{\boldsymbol{\sigma}}}\right)}{\frac{\partial g}{\partial \bar{\boldsymbol{\sigma}}} : \mathbf{C}^0 : \boldsymbol{l}(\bar{\boldsymbol{\sigma}}) - \frac{\partial g}{\partial \mathbf{r}} \cdot \frac{\partial \mathbf{r}}{\partial \boldsymbol{Y}}} \tag{22}$$

in which the following symbol

$$\boldsymbol{l}(\bar{\boldsymbol{\sigma}}) = \frac{\bar{\boldsymbol{\sigma}}}{\sqrt{\bar{\boldsymbol{\sigma}} : \bar{\boldsymbol{\sigma}}}} \tag{23}$$

has the physical meaning of the unit tensor parallel to the effective stress tensor.

2.2 Notes on integration algorithm

The concrete material state determination presents similarities to the classical plasticity return-mapping algorithm and it is quite straightforward.

The total strain is updated by the given incremental displacement field:

$$\boldsymbol{\varepsilon}_{n+1} = \boldsymbol{\varepsilon}_n + \nabla^{\mathrm{s}}(\Delta \mathbf{u}) \tag{24}$$

And the trial elastic state is computed as

$$\bar{\boldsymbol{\sigma}}_{n+1}^{trial} = \boldsymbol{C}^0 : (\boldsymbol{\varepsilon}_{n+1} - \boldsymbol{\varepsilon}_n^p) \tag{25}$$

If the plastic-damage criteria is respected there is evolution neither of the plastic strain, nor of the damage thresholds, nor of the damage parameters:

$$\boldsymbol{\varepsilon}_{n+1}^p = \boldsymbol{\varepsilon}_n^p \tag{26}$$

$$\boldsymbol{r}_{n+1} = \boldsymbol{r}_n \tag{27}$$

$$\boldsymbol{d}_{n+1} = \boldsymbol{d}_n \tag{28}$$

and therefore the trial effective stress can be confirmed

$$\bar{\boldsymbol{\sigma}}_{\boldsymbol{n+1}} = \bar{\boldsymbol{\sigma}}_{n+1}^{trial} \tag{29}$$

If the plastic-damage criteria is not respected it is necessary to use a return-mapping algorithm to update effective stress, plastic strain and plastic-damage thresholds such that the following equalities hold:

$$\bar{\boldsymbol{\sigma}}_{\boldsymbol{n+1}} = \boldsymbol{C}^0 : (\boldsymbol{\varepsilon}_{n+1} - \boldsymbol{\varepsilon}_{n+1}^p) \tag{30}$$

$$\boldsymbol{\varepsilon}_{n+1}^p = \boldsymbol{\varepsilon}_n^p + \beta E \frac{\langle \bar{\boldsymbol{\sigma}}_{\boldsymbol{n+1}} : \Delta \boldsymbol{\varepsilon} \rangle}{\bar{\boldsymbol{\sigma}}_{\boldsymbol{n+1}} : \bar{\boldsymbol{\sigma}}_{\boldsymbol{n+1}}} \boldsymbol{C}^{0\,-1} : \bar{\boldsymbol{\sigma}}_{\boldsymbol{n+1}} \tag{31}$$

$$g(Y_{n+1}^+, Y_{n+1}^-, r_{n+1}^+, r_{n+1}^-) = \left(\frac{Y_{n+1}^+}{r_{n+1}^+}\right)^2 + \left(\frac{Y_{n+1}^-}{r_{n+1}^-}\right)^2 - 1 = 0 \tag{32}$$

The solution of the previous nonlinear equations requires an iterative scheme that can be solved by the Newton method using the elastoplastic damage tangent modulus of the Equation (22).

As a consequence the damage parameters can be calculated directly

$$\boldsymbol{d}_{n+1} = \boldsymbol{d}_{n+1}(\boldsymbol{r}_{n+1}, \boldsymbol{r}_0) \tag{33}$$

When the two alternative branches of the integration have been completed, the Cauchy stress is obtained from the following equation

$$\boldsymbol{\sigma}_{n+1} = (1 - \boldsymbol{d}_{n+1}) : \bar{\boldsymbol{\sigma}}_{\boldsymbol{n+1}} \tag{34}$$

3 VALIDATION EXAMPLE FOR CONCRETE MATERIAL

Two simple numerical examples are reported in order to show the ability of the concrete damage model in reproducing the typical concrete behavior for 1D cyclic tests under tensile and compressive solicitations.

3.1 Cyclic uniaxial compressive loading test

In Figure 2 the experimental results, taken from Sinha et al. [33], are plotted against the numerical results. This experiment was already selected by Faria et al. [29], among others, to validate their model. The concrete material properties assumed for the model are derived from those reported by the authors of the experimental study: the compressive peak strength f_c^- = 32 MPa, the Young modulus E = 26 GPa, the compressive uniaxial initial elastic threshold f_0^- = 15 MPa, the plastic strain coefficient β = 0.590. The numerical model is very capable in reproducing the concrete nonlinear behavior. When the initial elastic limit is passed, the plastic strain and the damage parameter increase. The hysteresis of the reloading loop cannot be simulated by the model because of the rate-independent elastic loading/unloading assumption but the progressive degradation of the secant modulus fits the loading/unloading test curves on average very well.

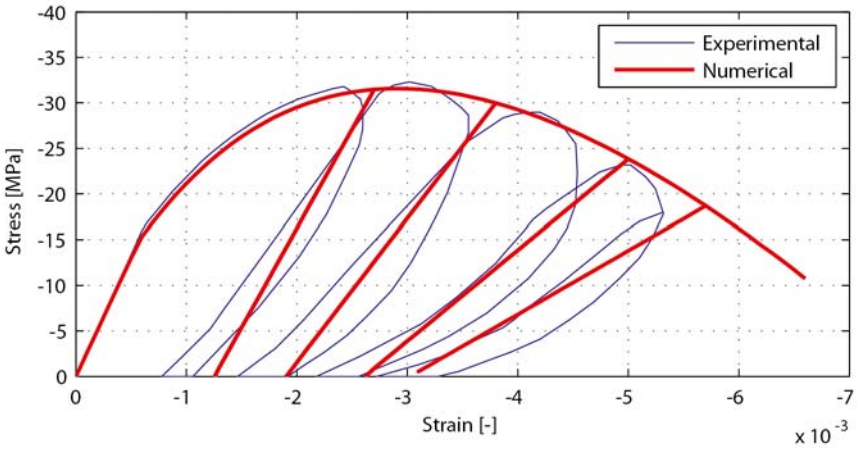

Figure 2: Cyclic uniaxial compressive loading test

The values reached by the negative damage parameter at the maximum strain of each cycle are depicted in Figure 3. In can be noted that its value is about 0.2 when the compressive peak strength is achieved. After a strength decay of about 25%, the damage parameter approaches 0.6. A damage value equal to 1.0 means that the strength and stiffness of the material are completely lost. It should be underlined that the damage parameters are positive scalar values

that cannot decrease since they depend on the maximum recorded damage threshold. This implies that a damage parameter remains constant during an unloading/reloading cycle until the maximum effective stress is exceeded again.

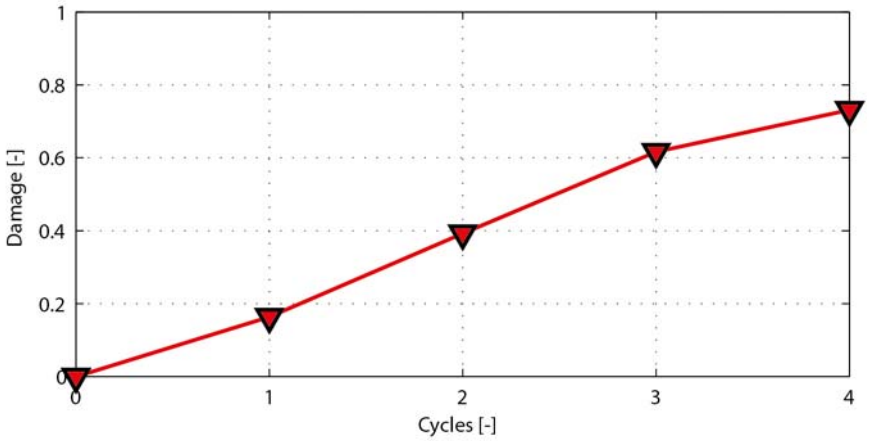

Figure 3: Negative damage index evolution

3.2 Cyclic uniaxial tensile loading test

The comparison between the experimental data (Gopalaratnam and Shah [34]) and the numerical results by means of a simple element patch, 82.6 x 82.6 mm, is illustrated in Figure 4. Also Lee and Fenves [17] chose this test to showcase their plastic-damage model. The degradation of stiffness is simulated at each unloading/reloading cycle as well as the softening behavior.

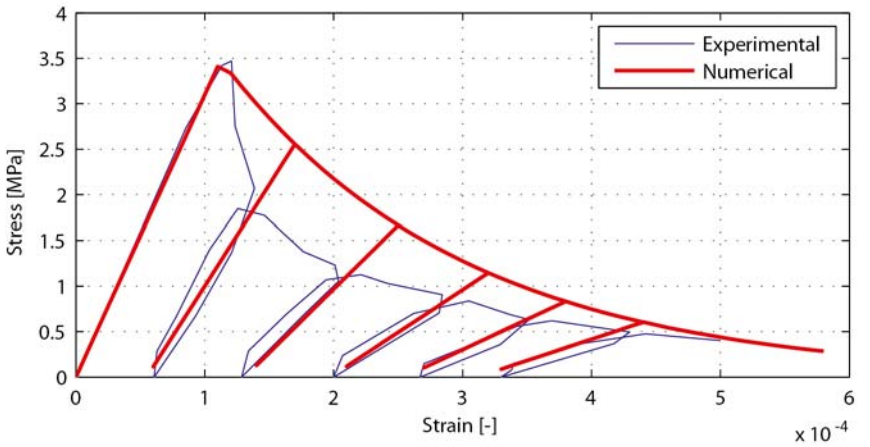

Figure 4: Cyclic uniaxial tensile loading test

Attention should be focused on the residual strain after complete unloading. In fact the residual strain consistently increases even for relatively high strain and very low residual tensile concrete strength. The numerical model can capture very effectively this effect though the plasticity extended in the present work also for tensile concrete stresses. The residual strains in tension are quite important because they affect crack closure state at loading reversals and they becomes particularly evident for cyclic shear tests of reinforced concrete membranes.

On the contrary, the gap between the experimental curve and the numerical one immediately after the peak strength does not condition the effectiveness of the model for the purposes of the present work because of two reasons: the difference of the two curves is relatively insigni-

ficant in terms of dissipated energy having the concrete material a very low tensile peak strength compared to the compressive one; the post crack behavior for reinforced concrete elements subjected to tension is characterized by the steel response and by the narrow tension stiffening effect.

The evolution of the positive damage parameter is shown in Figure 5. The damage parameter increases drastically at the beginning of the softening branch and then it approaches the unit asymptotically since the depletion of the fracture energy take place at strains much larger than the elastic limit.

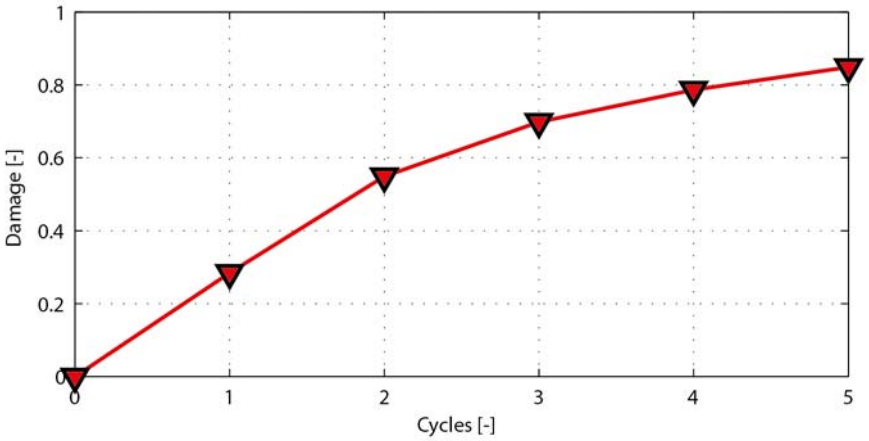

Figure 5: Positive damage index evolution

4 R/C MEMBRANE MODEL

The general three-dimensional concrete model has been developed in a plane stress state to represent the behavior of concrete panels.

Several choices are possible in order to reproduce the reinforcements. The simplest model considers the use of different finite elements for the reinforcing bars joining the concrete panels at the nodes (discrete approach). The main drawbacks of this choice are the need of introducing a steel element for each reinforcement position and the difficulty of introducing bars inclined differently respect to the panel mesh.

The proposed model considers the superposition of different material models to create the membrane model (embedded approach). Thus the reinforcements shall be represented as smeared since the overall behavior of the membrane shall comply with the panel kinematic. As a result the equivalence of the total strains of the different material is imposed. From the physical point of view this is equal to assume a perfect bond between concrete and reinforcing steel. Each steel layer can reproduce the behavior of a set of bars aligned to a generic direction respect to the element principal axis. As a simple generalization a steel layer can simulate the response of a reinforcement net with bars disposed in two orthogonal directions.

An important benefit of the membrane model is the possibility to reproduce all possible reinforcement configurations by simply adding the appropriate number of layers.

The model could be further extended to take into account the bond slip between the two materials at the cost of additional computational effort.

If a steel layer represents one set of parallel rebars, it has an uniaxial stress response in the direction of the bars. On the contrary, a net with bars in two orthogonal directions is simulated by a biaxial orthotropic stress response.

In the first case, the reinforcing layer state determination starts with the projection of the generic total strain tensor in the direction of the bars. Without losing in generality that direction is denoted by its cosine directors $\boldsymbol{u}$.

The total strain along the steel bar is easily obtained as:

$$\varepsilon_{\varphi} = \boldsymbol{\varepsilon}\, \boldsymbol{u} \cdot \boldsymbol{u} \tag{35}$$

that is used to compute the uniaxial steel material state determination by using the reinforcement constitutive law. In the present work the Menegotto-Pinto law with the isotropic hardening introduced by Filippou et al. [30] has been profitably selected for its ability to evaluate precisely the hysteretic behavior of the reinforcing steel.

The material state in terms of steel stress and tangent modulus are therefore re-projected in the original element reference frame:

$$\boldsymbol{\sigma}_s = \sigma_{\varphi}(\boldsymbol{u} \otimes \boldsymbol{u}) \tag{36}$$

$$\boldsymbol{C}_s = C_{s,\varphi}(\boldsymbol{u} \otimes \boldsymbol{u} \otimes \boldsymbol{u} \otimes \boldsymbol{u}) \tag{37}$$

These layer responses are added to those coming from the other concrete and steel layers. It can be underlined that the membrane model can be applied to any two-dimensional finite element. The authors have carried out several analyses running different elements i.e. four-node and nine-node quadrilateral and six-node triangular.

5 QUASI-STATIC EXAMPLES FOR THE R/C MEMBRANE MODEL

5.1 Examples of deep beams

The well known reinforced concrete beams tested by Leonhardt and Walther [35] are selected to validate the proposed model. Table 1 summarizes their geometry and the reinforcing steel. They are simply supported beams with two concentrated vertical loads symmetric respect to the beam midspan. The beams are characterized by the absence of shear reinforcement and a constant longitudinal reinforcement ratio of $\rho = 2.0\%$.

Beam ID	*L* (mm)	*a* (mm)	*h* (mm)	*b* (mm)	*a/d*	ρ (%)
T4	1700	670	320	190	2.5	2.0
T5	1950	810	320	190	3.0	2.0
T6	2350	1080	320	190	4.0	2.0
T7	3100	1350	320	190	5.0	2.0
T8	3600	1620	320	190	6.0	2.0
T9	5800	1890	320	190	7.0	2.0
T10	4700	2160	320	190	8.0	2.0

Table 1: geometry and reinforcement of the beams

The shear span-to-depth ratio a/d conditioned the experimental failure mode: flexural failure took place for high ratios while shear failure occurred for low ratios. In particular the transition from flexural to shear failure can be distinguished for $a/d = 6$.

The experimental setup has been numerically simulated. The constitutive laws of the concrete and steel have been calibrated using the parameters of Table 2, starting from the material mechanical properties of the specimens [35].

In Figure 6 the experimental failure loads are compared with the one related to the theoretical flexural strength and with those obtained by the numerical membrane model. The good

agreement between the experimental and the numerical values confirms the accuracy of the non linear model.

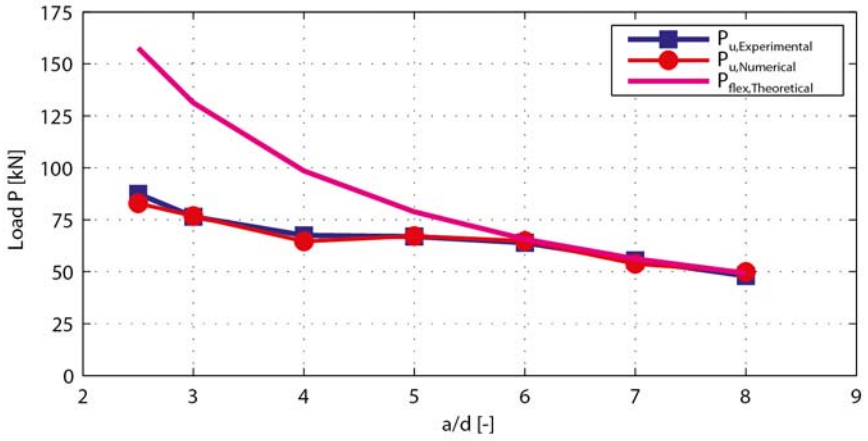

Figure 6: Comparison between experimental and numerical results for the failure load vs. span to depth ratio

Concrete		Reinforcing steel	
Young modulus	36 GPa	Young modulus	190 GPa
Poisson coefficient	0.15	Yielding strength	360 MPa
1D compr. strength	28.0 MPa	Hardening modulus	3 GPa
2D compr. strength	33.6 MPa		
1D compr. elastic threshold	18.2 MPa		
1D tensile strength	2.0 MPa		

Table 2: material model parameters used for the numerical analysis

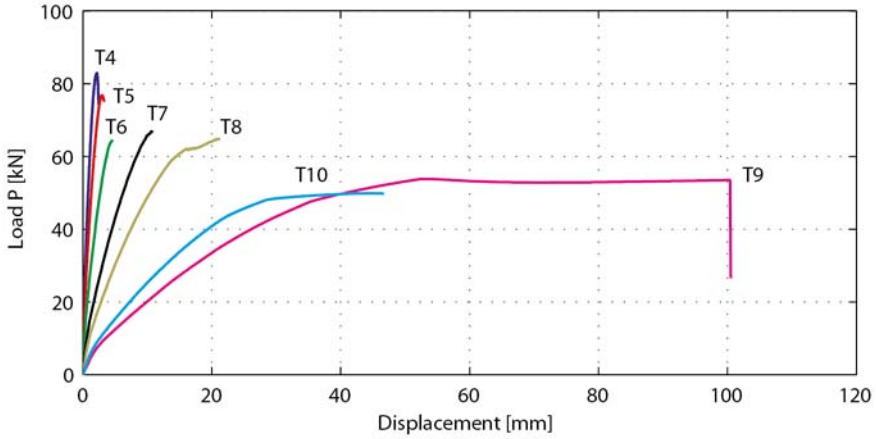

Figure 7: Numerical load vs. displacement curves of the beams

Figure 7 shows the load vs. displacement curves obtained by the numerical models. The corresponding experimental curves were not reported by the test authors.

The curves for the beam T9 and T10 show high plastic deformations, after the longitudinal bar yielding characteristic of a flexural failure mode, whereas the remaining beams with lower span-to-depth ratios suffered shear failure as the abrupt termination of their curves demonstrates.

The specimen T4, with the lowest a/d =2.5, showed a so-called "shear compression failure" that is the crushing of upper compressed concrete area due to the progressive development of the diagonal cracks induced by shear stresses under the point of load application. The experimental failure occurred at the load of 87.5 kN, while the numerical simulation provides a corresponding value of 83 kN. This beam characterizes the deepest point for the "shear valley" of the specimen set having a reduction of the failure moment equal to the 53% of the theoretical flexural value.

5.2 Example of R/C panels

The new model has been validated by comparison with several experimental results on reinforced concrete panels from the literature.

In particular all the specimens presented by Mansour and Hsu [8] have been considered. The comparison has been even more significant thanks to the kind availability of Professor Hsu to produce the experimental measured data upon request.

These R/C panels were submitted to increasing amplitude cyclic load reversals of pure shear solicitations in their mid-plane by means of the "Universal Panel Tester" at the University of Huston (Texas, USA). The loads had been applied uniformly on the panels edges.

The reinforcement had been placed in different directions respect to the solicitation principal axes and with variable ratios for each panels.

Table 3 recalls the main panel properties while the exhaustive specimen description can be found in the work of the test authors [8]. The symbols assume the following meanings:

- f'_c compressive strength of cylindrical concrete specimen;
- α_2 angle between the vertical specimen direction and the l reinforcing bar one;
- ρ_l reinforcement ratio in l direction;
- f_{ly} tensile yielding strength of reinforcing bar in l direction;
- ρ_t reinforcement ratio in t direction (at 90° respect to l direction);
- f_{ty} tensile yielding strength of reinforcing bar in t direction.

The specimens had been loaded through cyclic load reversals under load control before the yielding strength and under displacement control for further cycles. During this last part the shear deformation has been used as controlling parameter and the shear strain values are multiple of the yield shear strain.

Panel ID	f'_c	α_2	ρ_l	f_{ly}	ρ_t	f_{ty}
CA2	45.0	45.0°	0.0077	424.1	0.0077	424.1
CB3	48.0	45.0°	0.0170	425.4	0.0077	424.1
CD3	47.0	68.2°	0.0130	425.3	0.0130	425.4
CF2	44.0	79.8°	0.0056	424.1	0.0056	424.1
CE3	50.0	90.0°	0.0120	425.4	0.0120	425.4

Table 3: Mechanical properties of the panel materials

The pure shear solicitation had been applied by imposing normal stresses equal in absolute value but opposite in sign along the vertical and the horizontal directions of the specimens.

The applied loads and the panel averaged strains had been measured by load cells placed on each jack and by displacement transducers over a length traversing several cracks.

In order to verify the accuracy of the numerical model and thanks to the availability of the experimental data, the numerical results are compared to the specimen ones.

In sake of brevity the results of one panel for each series of bar inclination are presented in terms of shear stress vs. shear strain response (see from Figure 8 to Figure 12).

The specimens identified by CA2, CB3, CD3, CF2, CE3 are considered in decreasing order of angle amplitude between the rebar directions and the principal stress ones.

The letter A stands for an angle between the steel bar orientation and the vertical principal stresses equal to 45°. The specimen CA2 has equal reinforcement ratios of 0.0077 in both the net directions. The experiment authors have reported that an "out of stroke" happened at the end of the test. That inconvenience had inevitably conditioned the data recorded in the last load cycles both for positive and negative shear stresses (see Figure 8). Thus the strength decay, in the last cycles, was not caused by the panel failure but rather by the insufficient push of the jacks. It is confirmed by the same authors when they admit that the ductility of the panel CA2 shall be considered higher than that recorded because the collapse of the panel was not reached due to "equipment limitations".

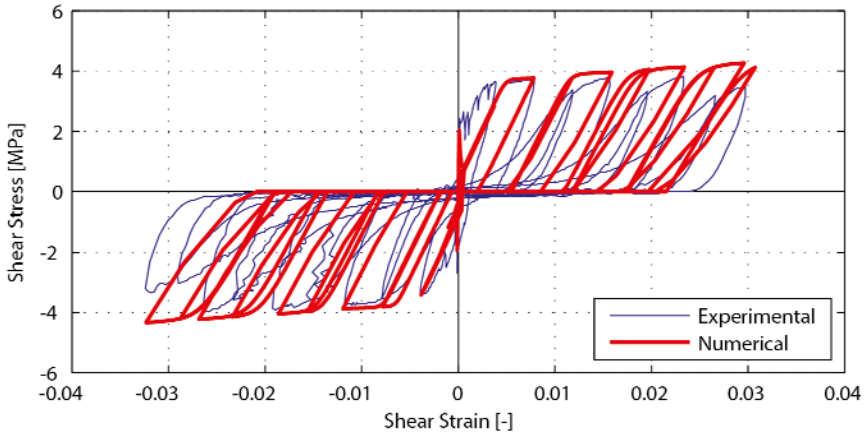

Figure 8: Comparison between experimental and numerical results of the specimen CA2 for shear stress vs. shear strain response

The behavior of the specimen has been rather correctly simulated in terms of fracture load, shear strength, ductility of the panel, pinching effect of the hysteretic curve.

Since the bar net is inclined of 45° respect to the principal stress directions, all the reinforcements bear the tensile loads in both the principal directions with equal stresses. This leads to a progressive delay in recovering the stiffness and the strength at load reversals as far as the plastic strain increases. Even if the numerical model cannot account for the crack interlocking and the progressive stiffness recovering of the specimen, nonetheless it can fairly simulate the stiffness recovering in the average.

The tension stiffening effect does not seem to be captured by the numerical model, but also the experimental data appear to be definitely unstable.

The unloading stiffness of the model is lower than the specimen one after the yielding conditions. This evidence is likely due to the inability of the model to account for bar bond slip and bar dowel action effects.

The specimen CB3 has reinforcement ratios equal to 0.0077 and 0.0170 in the two rebar directions aligned again at 45° respect to the principal stress ones. The experiment authors did not have reported any inconvenience occurred during the test. The numerical model shows good results referring in particular to the cyclic response envelope that includes (see Figure 9): the initial stiffness, the yielding load, the peak strength and the compressive concrete failure. The unloading stiffness seems underestimated especially after the concrete crushing as for the previous example.

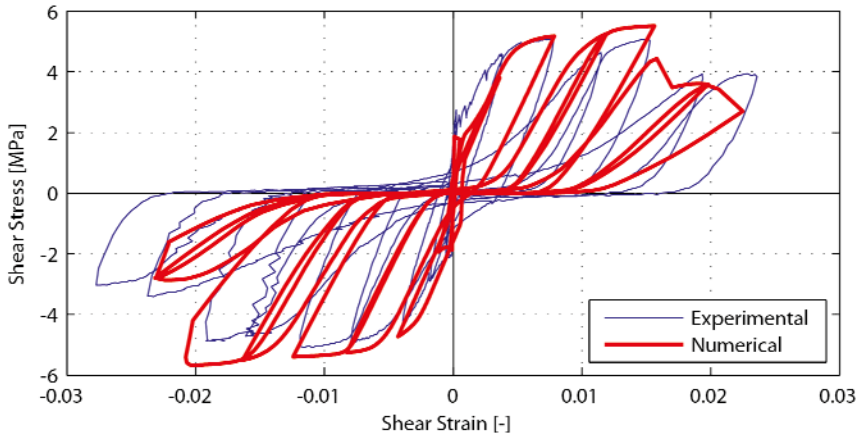

Figure 9: Comparison between experimental and numerical results of the specimen CB3 for shear stress vs. shear strain response

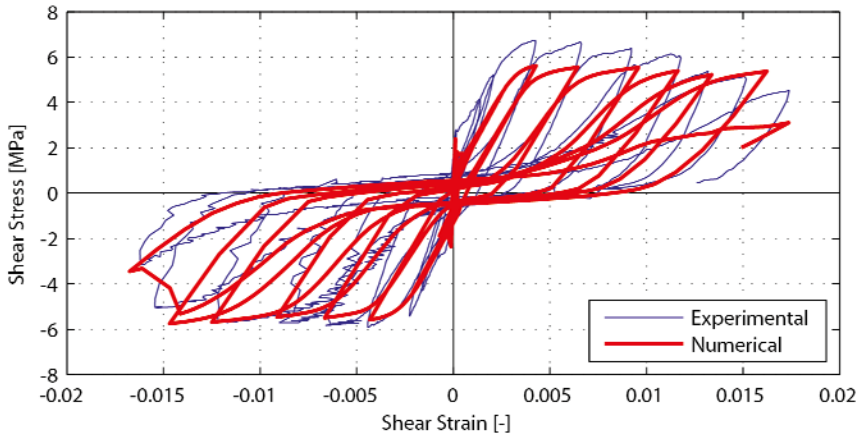

Figure 10: Comparison between experimental and numerical results of the specimen CD3 for shear stress vs. shear strain response

The specimen CD3 has the bar inclination angle equal to 68.2° and a reinforcement ratio of 0.0130 in both the net directions. The strength reduction of the specimen in the cycles can be attributed to the panel failure and the panel ductility had been accurately described. No comment was pointed out by the experimenters on the equipment functioning even though the strain transducers show a certain instability both in the loading and unloading cycle branches. The measured strength turned out to be markedly non symmetric for the positive and negative shear values. Such evidence is not justified by any specimen theoretical asymmetry and it can be caused by an unknown realization fault in the test geometrical configuration. The response of the numerical model is necessarily symmetric and it fits very well the envelope for the negative shear stresses being able to simulate the concrete cracking, the post-cracking loading stiffness, the yielding strength, the maximum ductility determined by the compressive concrete crushing and the pinching effects of the hysteretic curve. The panel progressive cracking phase does not seem to be fully captured even if the experimental data look quite asymmetric and partially unstable.

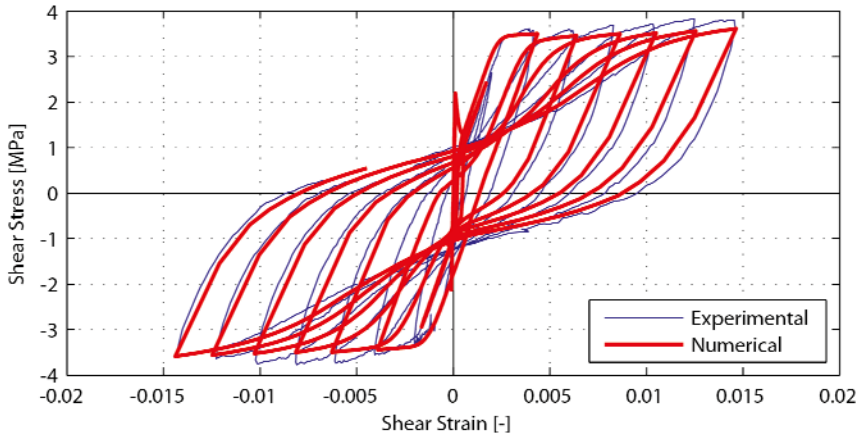

Figure 11: Comparison between experimental and numerical results of the specimen CF2 for shear stress vs. shear strain response

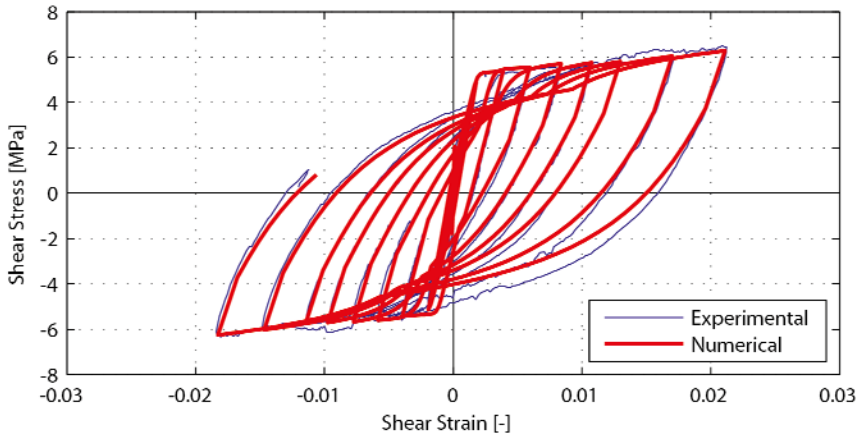

Figure 12: Comparison between experimental and numerical results of the specimen CE3 for shear stress vs. shear strain response

The CF2 panel is the only panel with an angle of 79.8° between the steel net and the principal stress axes and the reinforcement ratio is 0.0056 in both the directions. The numerical model describes accurately the specimen behavior being able to catch the cracking load, the yielding strength, the ductility and the dissipation capacity (see Figure 11). As it is shown by the present example, but it can be noted in general, the proposed model provide an estimation of the dissipated energy that is lightly less than the real one. This fact might be caused by the hypothesis of disregarding the bond slip phenomenon and by considering only the axial response of the reinforcing bars. In compensation the numerical procedure is quite efficient and it is suitable for application to large scale structures. Furthermore a light underestimation of the dissipated energy is pro-safety in executing nonlinear seismic analyses.

The example of the last series is the panel CE3 which has the reinforcing bars parallel to the applied principal stresses and a symmetric reinforcement ratio equal to 0.0120. The test authors reported that the ductility of the specimen could not have completely exploited since the maximum lengthening of the jacks was reached. The experimental data show an unexplained minor asymmetry concerning the last two reloading negative braches of the global response as it can be seen from Figure 12. Nonetheless the example show clearly how the numerical model can reproduce precisely the recorded panel behavior in all its features such

as, for instance, the yielding strength and the following hardening behavior, the unloading stiffness and the residual deformation at load reversals and energy dissipation capacity.

In order to further investigate in the response of the numerical model for the last example, other two responses are herein presented: the vertical strain vs. horizontal strain curve and the vertical normal stress vs. the corresponding vertical strain one (see. Figure 13 and Figure 14).

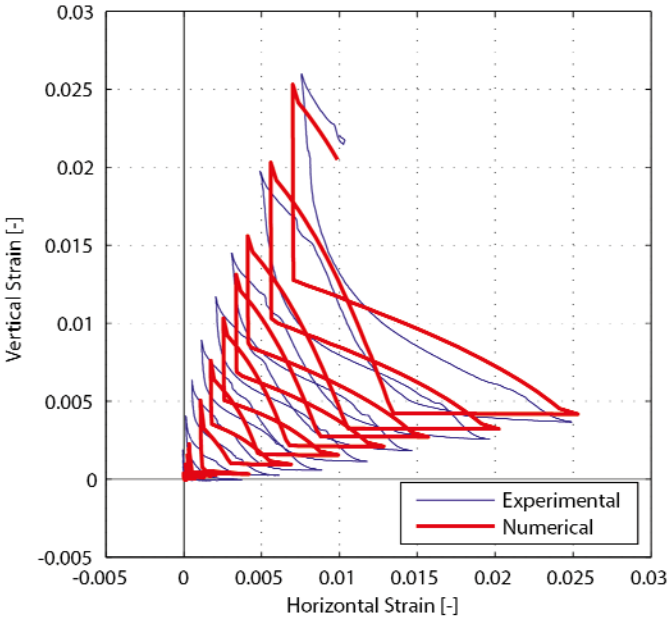

Figure 13: Comparison between experimental and numerical results of the specimen CE3 for vertical strain vs. horizontal strain response

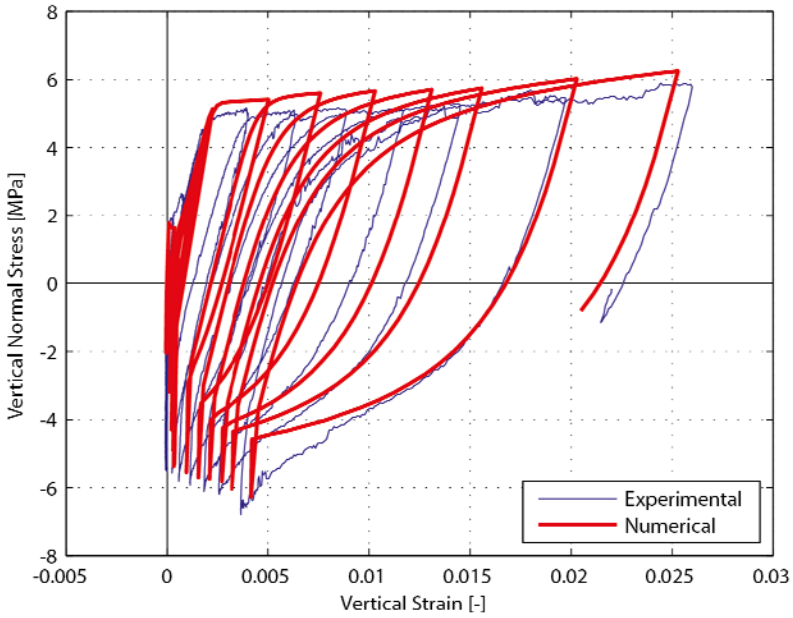

Figure 14: Comparison between experimental and numerical results of the specimen CE3 for vertical normal stress vs. vertical strain response

It can be noted that the axial strains are evaluated with high accuracy. This shall not be considered an automatic consequence of imposing the shear strain in the cycles after the panel yielding. In fact the shear strain compels only the difference between the positive and the negative axial strains but not their values separately.

The progressive expansion of the panel due to the accumulation of plastic strain is correctly captured by the proposed model. The gap between the two curves visible in the central part between following tips is explained by the sudden closure of the cracks in the numerical model, whereas the experiment exhibits a progressive stiffness recovery due to local effects occurring when the opposite irregular surfaces of a crack move close again. This fact is evident also comparing the vertical stress-strain response depicted in Fig. 14.

It is important to notice that the strain data are computed from dilatation measures over several crack distances leading to averaged values while the numerical response is punctual and would properly represent the behavior of a cracked section.

6 CONCLUSIONS

- An efficient two parameter concrete plastic damage model has been developed that is suitable for the simulation of large scale structural models with RC panels.
- The validation examples have confirmed the ability of the concrete material to simulate the nonlinear cyclic behavior of concrete under tensile and compressive strains.
- A straightforward formulation of a R/C membrane model has been proposed by superimposing different materials, concrete and reinforcing steel, to create a single membrane model with smeared reinforcement of general orientation.
- The well-known Leonhardt beams are simulated to point out the efficiency of the model in reproducing the transition from flexural to shear failure mode for deep beams. The membrane model has been able to correctly predict the “shear valley”.
- A second set of simulation of R/C panel is carried out. The examples show clearly the ability of the proposed model to reproduce the main features of the experimental panel behavior such as: the yield strength, the subsequent hardening/softening behavior, the residual deformation at load reversals and energy dissipation capacity.

ACKNOWLEDGEMENT

The authors warmly thank Professor T.T.C. Hsu for making available the experimental data obtained in the Structural Research Laboratory at the University of Houston (Texas, USA).

REFERENCES

[1] F. Leonhardt, E. Mönnig, *Vorlesungen über Massivbau. Teil 2: Sonderfälle der Bemessung im Stahlbetonbau*. Springer Verlag, 1975.

[2] Z.P. Bazant, T. Tsubaki, T.B. Belytschko, Concrete reinforcing net - safe design. *Journal of the Structural Division ASCE*, **106**, 1899-1906, 1980.

[3] F. Vecchio, M.P. Collins, *Response of reinforced concrete to in-plane shear and normal stresses*. Department of Civil Engineering, University of Toronto, 1982.

[4] S.B. Bhide, M.P. Collins, *Reinforced concrete elements in shear and tension*. Department of Civil Engineering, University of Toronto, 1987.

[5] N. Ohomori, H. Tsubota, N. Inoue, K. Kurihara, S. Watanabe, Reinforced concrete membrane elements subjected to reversed cyclic in-plane shear stress. *Nuclear Engineering and Design*, **115**, 61-72, 1989.

[6] T.N. Salonikios, A.J. Kappos, I.A. Tegos, G.G. Penelis, Cyclic load behavior of low-slenderness reinforced concrete walls: Design basis and test results. *ACI Structural Journal*, **96**, 649-660, 1999.

[7] J.H. Thomsen, J.W. Wallace, Displacement-based design of slender reinforced concrete structural walls - experimental verification, *Journal of Structural Engineering ASCE*, **130**, 618-630, 2004.

[8] M. Mansour, T.T.C. Hsu, Behavior of reinforced concrete elements under cyclic shear. I: experiments. *Journal of Structural Engineering ASCE*, **131**, 44-53, 2005.

[9] C. Greifenhagen, P. Lestuzzi, Static cyclic tests on lightly reinforced concrete shear walls. *Engineering Structures*, **27**, 1073-1712, 2005.

[10] D. Darwin, D. Pechnold, Analysis of RC shear panels under cyclic loading. *Journal of the Structural Division ASCE*, **102**, 355-369, 1976.

[11] N. Bicanic, O.C. Zienkiewicz, Constructive model for concrete under dynamic loading. *Earthquake Engineering and Structural Dynamics*, **11**, 689-710, 1983.

[12] Y. Ohtani, W.F. Chen, Multiple hardening plasticity for concrete materials. *Journal of Engineering Mechanics ASCE*, **114**, 1890-1910, 1988.

[13] Z.P. Bazant, B. Oh, Crack band theory for fracture of concrete. *Materials and Structures*, **16**, 155-177, 1983.

[14] J. Cervenka, V.K. Papanikolaou, Three dimensional combined fracture-plastic material model for concrete. *International Journal of Plasticity*, **24**, 2192-2220, 2008.

[15] L.M. Kachanov, *Introduction to continuum damage mechanics*. Martinus Nijhoff Publisher, 1986.

[16] J. Mazars, G. Pijaudier-Cabot, Continuum damage theory - application to concrete. *Journal of Engineering Mechanics ASCE*, **115**, 345-365, 1989.

[17] J. Lee, G. Fenves, Plastic-damage model for cyclic loading of concrete structures. *Journal of Engineering Mechanics ASCE*, **124**, 892-900, 1998.

[18] R.H. Graves, K.N. Derucher, Interface smeared crack model analysis of concrete dams in earthquakes. *Journal of Engineering Mechanics ASCE*, **113**, 1678-1693,1987.

[19] F.J. Vecchio, M.P. Collins, The modified compression-field theory for reinforced-concrete elements subjected to shear. *ACI Structural Journal*, **83**, 219-231, 1986.

[20] F.J. Vecchio, Reinforced concrete membrane element formulations. *Journal of Structural Engineering ASCE*, **116**, 730-750, 1990.

[21] M.A. Polak, F.J. Vecchio, Reinforced-concrete shell elements subjected to bending and membrane loads. *ACI Structural Journal*, **91**, 261-268, 1994.

[22] M. Mansour, T.T.C. Hsu, Behavior of reinforced concrete elements under cyclic shear. II: Theoretical model. *Journal of Structural Engineering ASCE*, **131**, 54-65, 2005.

[23] L.N. Lowes, A. Altoontash, Modeling reinforced-concrete beam-column joints subjected to cyclic loading. *Journal of Structural Engineering ASCE*, **129**, 1686-1697, 2003.

[24] L.M. Massone, J.W. Wallace, Load – deformation responses of slender reinforced concrete walls. *ACI Structural Journal*, **101**, 103-113, 2004.

[25] L.M. Massone, K. Orakcal, J.W. Wallace, Shear - flexure interaction for structural walls. *ACI Special Publication SP-236: Deformation Capacity and Shear Strength of Reinforced Concrete Members Under Cyclic Loading*, Editor Adolfo Matamoros & Kenneth Elwood, 127-150, 2006.

[26] A. Saritas, F.C. Filippou, Inelastic axial-flexural-shear coupling in a mixed formulation beam finite element. *International Journal of Non-Linear Mechanics*, **44**, 913-922, 2009.

[27] P. Martinelli, F.C. Filippou, Simulation of the shaking table test of a seven-story shear wall building. *Earthquake Engineering and Structural Dynamics*, **38**, 587-607, 2009.

[28] R. Scotta, R. Vitaliani, A. Saetta, E. Oñate, A. Hanganu, A scalar damage model with a shear retention factor for the analysis of reinforced concrete structures: theory and validation. *Journal of Computer and Structures*, **79**, 737-755, 2001.

[29] R. Faria, J. Oliver, M. Cervera, A strain-based plastic viscous-damage model for massive concrete structures. *International Journal of Solids and Structures*, **35**, 1533-1558, 1998.

[30] F.C. Filippou, E.P. Popov, V.V. Bertero, *Effects of Bond Deterioration on Hysteretic Behavior of Reinforced Concrete Joints*. Earthquake Engineering Research Center, University of California, Berkeley, 1983.

[31] J.W. Ju, On energy-based coupled elastoplastic damage theories: constitutive modeling and computational aspects. *International Journal of Solids and Structures*, **25**, 803-833, 1989.

[32] J.Y. Wu, J. Li, R. Faria, An energy release rate-based plastic-damage model for concrete. *International Journal of Solids and Structures*, **43**, 583-612, 2006.

[33] E. Sinha, K. Gerstle, L. Tulin, Stress-strain relations for concrete under cyclic loading. *Journal of the ACI*, **62**, 195-210, 1964.

[34] V.S. Gopalaratnam, S.P. Shah, Softening response of plain concrete in direct tension. *Journal of the ACI*, **82**, 310-323, 1985.

[35] F. Leonhardt, R. Walther, Einfluss des Momenten-Schub-Verhältnises auf die Schubtragfähigkeit bei Rechtenbalken ohne Schubbewehrung unter Einzel- und Gleichlast. *Beton und Stahlbeton*, **2**, 1962.

[36] R. Scotta, D.A. Talledo, L. Tesser, R. Vitaliani, Non-Linear Behaviour Modelling of RC Panels Subjected to In-Plane Loads. *IV European Conference on Computational Mechanics*, paper n. 1065, Paris, May 16-21, 2010.